Feature

Chris M. Hymel, Malcolm H. Skolnick,
Ron A. Stubbers, and Michael E. Brandt

Temporally Advanced Signal Detection: A Review of the Technology and Potential Applications

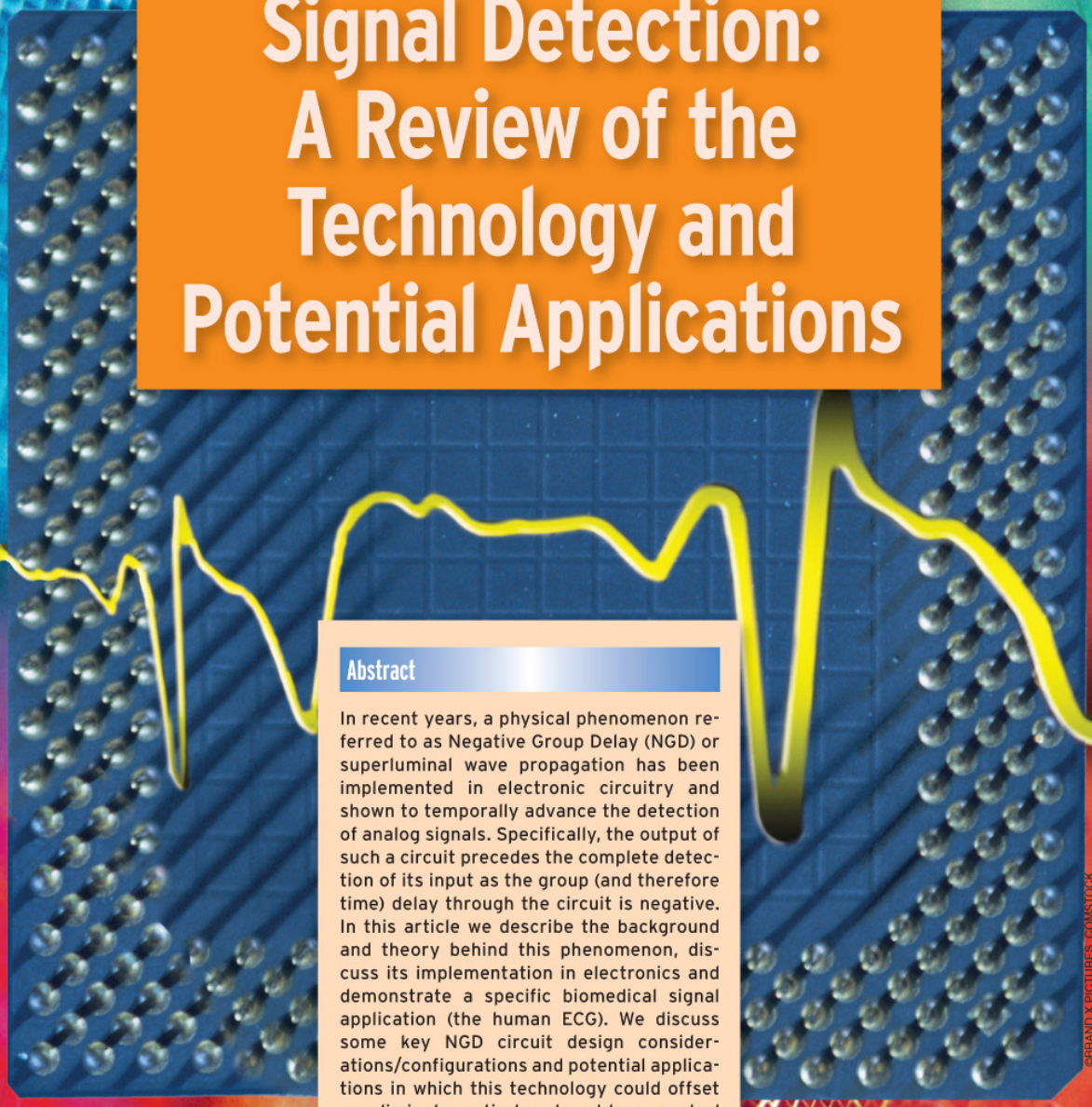

Abstract

In recent years, a physical phenomenon referred to as Negative Group Delay (NGD) or superluminal wave propagation has been implemented in electronic circuitry and shown to temporally advance the detection of analog signals. Specifically, the output of such a circuit precedes the complete detection of its input as the group (and therefore time) delay through the circuit is negative. In this article we describe the background and theory behind this phenomenon, discuss its implementation in electronics and demonstrate a specific biomedical signal application (the human ECG). We discuss some key NGD circuit design considerations/configurations and potential applications in which this technology could offset or eliminate entirely, closed-loop control system delays.

Digital Object Identifier 10.1109/MCAS.2011.941076
Date of publication: 25 August 2011

1531-636X/11/$26.00©2011 IEEE

I. Introduction

Negative Group Delay (NGD) refers to a phenomenon whereby an electromagnetic wave traverses a dispersive material or electronic circuit in such a manner that its amplitude envelope (its "group") is temporally *advanced* through the media rather than undergoing a temporal delay. This indicates that a portion of the wave is traveling superluminally, i.e., at a speed greater than c, the velocity of light in a vacuum (300,000 km/s). The effect of NGD is that a frequency bandlimited waveform emerging from a medium is actually shifted back in time with respect to the same wave entering into the medium – a highly counterintuitive but nevertheless real and observed effect.

In the research literature, the terms Superluminal Wave Propagation and Faster-than-Light propagation have been used to describe this phenomenon [1–7,15,23]. The use of these particular labels has resulted in some controversy among engineers and scientists investigating the phenomenon (discussed further in Section IIC below). The overall effect of NGD on signal propagation may more accurately and appropriately be referred to as Temporally Advanced Signal Detection (TASD). Our group has also used the term Signal Advance (SA) when referring to specific embodiments (e.g., in circuitry) and applications of the associated technology.

The effect is associated with a number of wave-media interaction mechanisms. These include anomalous dispersion, evanescent propagation, and wave interference. It is regularly observed to occur in ultrafast laser systems as well [7] and has also been demonstrated in electronics with lower frequency signals [3,4,5]. A number of applications have been described in the literature in which TASD purportedly improves operational efficiency and system performance in several domains including transistor-transistor communication [3], signal sampling and processing [8], feed-forward amplification [9], microwave applications [10] and signal cable transmission [11]. As of this writing, no references in the literature have yet been found reporting biomedical signal applications of TASD, nor of applications in closed-loop control/interventional systems.

In this article we report some of the findings on TASD modeled and implemented in electronic circuitry applied to a variety of constructed-simulated waveforms and to human electrocardiograph (ECG heart beat) signals. Our focus here is on the implementation and potential applications of TASD in electronics. The article includes a background section discussing signal propagation and group velocity, and the theoretical basis for the phenomenon along with its causal implications. We follow this with a discussion of basic circuitry that exhibits the SA effect. We then review a number of studies on the subject. Practical considerations regarding signal conditioning, and cascaded/parallel SA circuit configurations are discussed as well.

A specific SA circuit we designed and developed using both SPICE circuit simulation software and mathematical modeling is discussed. The circuit's stability and transient response were analyzed and its characteristics in terms of gain, phase and group delay relative to frequency are provided. The SA circuit model designed for an appropriate frequency range is then tested using a series of simulated/constructed signals and single human heartbeat ECG records. The gain, temporal advance and output signal distortion analysis results are then described. Finally, we discuss potential applications of SA technology that could improve the general responsiveness of a broad range of both biomedical and non-biomedical applications.

II. Definitions, Theory and Background

Fig. 1 illustrates a standard top level black box system configuration showing a linear time invariant (LTI) "allpass" filter characterized by its impulse response function $h(t)$ with a continuous analog input signal $x(t)$ yielding output signal $y(t)$. The input and output are related through the convolution $y(t) = x(t) * h(t)$. The filter's gain as a function of frequency is $G(j\omega) = |H(j\omega)|$, where $H(j\omega)$ is its transfer function (the Fourier transform of $h(t)$). The filter's phase response is $\varphi = \arg(H(j\omega))$. Assuming $H(j\omega)$ is a continuous function of frequency ω, the filter's group delay is defined as the negative of the derivative of its phase with respect to frequency, or $\tau(\omega) = -d\varphi(\omega)/d\omega$ [13].

For frequencies in which $\tau(\omega) > 0$ (i.e., positive group delay), the output signal at those frequencies is a temporally delayed version of the input signal. Conversely, for frequencies in which $\tau(\omega) < 0$ (i.e., negative group delay), the output signal is, by definition, a temporally advanced version of the input signal. In this case it would appear that (at least) a portion of the filter's output signal precedes the complete detection of its input signal. This leads to the abovementioned contradiction regarding

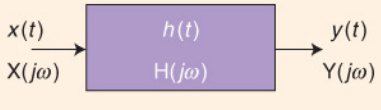

Figure 1. LTI allpass filter with input and output signals.

Chris M. Hymel (email: chymel@signaladvance.com), Malcolm H. Skolnick (email: mskolnick@signaladvance.com), Ron A. Stubbers (email: rstubbers@signaladvance.com) and Michael E. Brandt (email: mebrandt@signaladvance.com) are based in Houston, Texas.

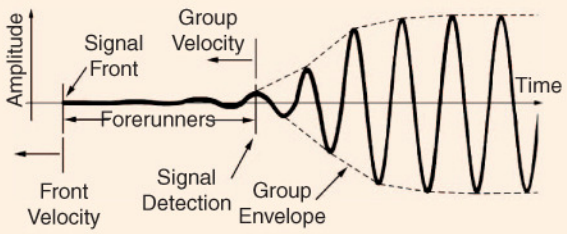

Figure 2. Waveform velocity components.

causality which we discuss in further detail below. First, we review the history and background of TASD with particular emphasis on wave physics.

In the early years of the twentieth century, the physicists Arnold Sommerfeld and Léon Brillouin [12] described a phenomenon in which a significant portion of the energy of an electromagnetic waveform (such as an optical signal or an electrical signal) appears to propagate through a dispersive medium (including various types of semiconductors) with superluminal velocity. The distance and speed could in fact be such that the waveform traverses the media with little or no time delay at all, or could actually even emerge from the media advanced in time relative to when the waveform entered into the media in the first place.

The manner with which waveforms traverse such media appears to be anomalous or counterintuitive. At first glance it seems that causality is violated as the waveform emerges from the medium before it has fully entered into it (i.e., the input signal has not yet been completely detected). It has been shown however that this is not the case – TASD in fact does not violate causality.

A. Components of Waveform Velocity

In order to understand this seemingly contradictory behavior it is important to point out that electromagnetic propagation is characterized by five unique waveform velocities as described by Brillouin [12]. These are

- *Phase velocity* – the speed at which the phase of any one spectral frequency component of the wave travels.
- *Group velocity* – the speed at which the variations in the shape of the wave's amplitude (known as the modulation or envelope of the wave) propagates.
- *Front velocity* – the speed of an abrupt signal discontinuity (signal abruptly turned on or off). It is considered as the very beginning of the signal in time, and it never exceeds c.
- *Energy velocity* – the speed of energy transfer.
- *Signal velocity* – the speed of information transfer, which, under various conditions, may be equivalent to one or more of the above four velocities.

According to Brillouin, the "front velocity will correspond to the speed at which the first, extremely small (perhaps invisible) vibrations will occur, while the signal velocity yields the arrival of the main signal, with intensities on the order of the magnitude of the input signal." [12].

Typically, the signal velocity is equivalent to both the group and energy velocities. While the front velocity cannot exceed the speed of light, in special cases (e.g. media or circuitry that amplifies the initial or anterior-most portion of a waveform and attenuates the posterior portion), "… the group velocity … can be greater than the velocity of light *c*, can be infinite and even negative!" [12]. That is, the detection of a pulsatile input or extended-in-time waveform at the output of the medium can precede its *complete* detection of the waveform at the input.

During the time interval between the arrival of the wavefront (front velocity) and the actual detection of the group waveform, electromagnetic energy begins to propagate through the medium, the magnitude of which is not detectable until the oscillations achieve sufficient amplitude (Fig. 2). These very early, very low energy (typically undetected) perturbations (referred to as "forerunners" by Brillouin) actually contain sufficient information to reproduce a temporally advanced signal.

TASD may be accomplished by using a high-gain electronic oscillator to amplify the earliest waveform deflections [1,3,15]. A temporal advance may not, however exceed the signal front establishing a theoretical signal detection or group velocity advance upper limit [1,3,12].

Electrophysiological (and many other types of) signals are typically characterized by a waveform amplitude envelope that propagates at the group velocity. Thus, for most bioelectric waveforms (examples include the electrocardiogram, or ECG, the electroencephalogram or EEG and the electromyogram or EMG), the signal velocity itself is equivalent to the group velocity.

B. System Response Functions

To illustrate the relationship between phase and group delay, the gain, phase and group delay responses relative to frequency of a simple two-stage SA circuit model designed to temporally advance a 0.3 Hz sine wave are shown in Fig. 3 (the model was also physically implemented in electronic circuitry) [13]. Viewing the gain function in Fig. 3a, we see that this particular circuit functions as a lowpass filter. As such, its transfer function will differentially alter the gain of the output signal with respect to its input over a spectral range of 0.1 to 1.0 Hz, as shown.

For frequencies in which the phase (Fig. 3b) has a negative slope (less than 0.275 Hz and greater than 0.325 Hz), the group delay (Fig. 3c) is positive. For frequencies in which the phase has a positive slope

(between approximately 0.275 Hz and 0.325 Hz) the group delay is negative, decreasing very rapidly to just under −450 ms (or, stated alternatively, a temporal group advance of +450 ms).

Note that the group delay response is decidedly not constant over the frequency range shown in Fig. 3c. If a signal comprised of multiple frequencies in this range were applied to this circuit, its frequency components would undergo differential temporal delay and/or advance. This would mean that the circuit's output signal would be (at least) a moderately distorted version of its input, the extent of this distortion being dependent upon the degree of non-constancy of both the circuit's gain and group delay responses.

Fig. 4 shows results of an experiment performed by passing a Gaussian shaped waveform having an effective frequency of exactly 0.3 Hz through this two-stage SA circuit. Note that the peak of the output signal actually precedes the *complete* detection of the input signal peak by approximately 450 ms as predicted by the group delay graph (Fig. 3c). Note also that the shape of the output signal is almost identical to that of the circuit's input signal (the overall output has been uniformly amplified).

However, the non-constancy of the gain and group delay responses (Fig. 3) severely limits this circuit's potential utility to temporally advance an input signal consisting of broader spectral content. due to the distortion of the input noted above. To address this deficiency, we developed and tested an SA circuit that displays both a constant gain and negative group delay over a frequency band relevant for a variety of biomedical as well as non-biomedical signals.

C. TASD and Causality

As TASD implies superluminal wave velocity [3,5,6] it raises a question as to whether or not causality is violated in media or electronic systems that demonstrate the phenomenon. This question was addressed in studies in which the input signal was suddenly discontinued. This resulted in a simultaneous rather than advanced discontinuity (signal or waveform abruption) in the output demonstrating that a causal relationship between the input and output waveforms does indeed exist [1,3,5]. The causality issue was further examined in a study in which detection of the temporally advanced output peak was used as a trigger to abruptly discontinue the input signal before reaching its peak amplitude [2]. This resulted in a damped oscillation in the temporally advanced output waveform, again demonstrating that causality is not violated in such media/systems.

TASD essentially imparts a phase shift to an input signal thereby advancing its detection without violating causality. TASD has been demonstrated with both narrow and wideband audio signal inputs in which, over a band-limited spectral range, the phase has a positive linear slope with respect to frequency [5]. The remainder of this article describes implementation of TASD in electronic circuitry only.

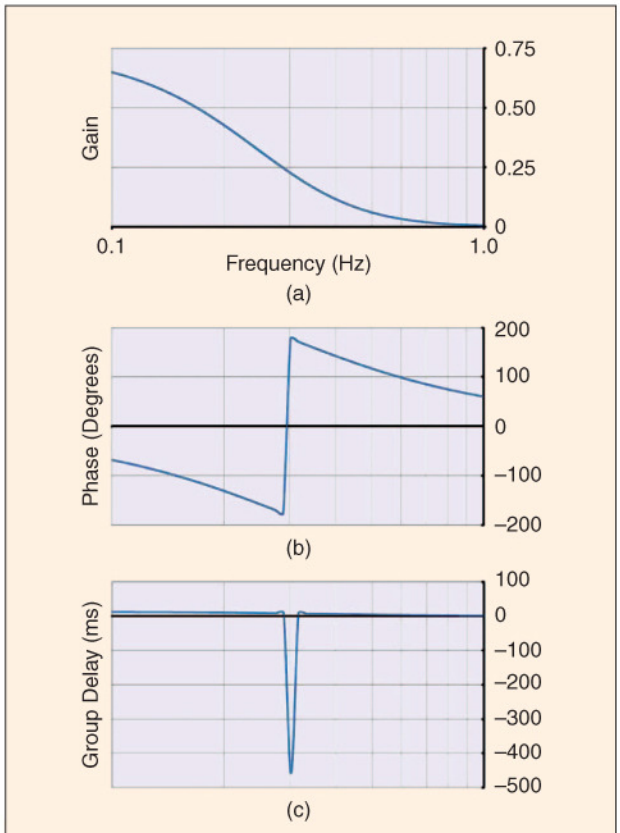

Figure 3. Gain, phase and group delay relative to frequency.

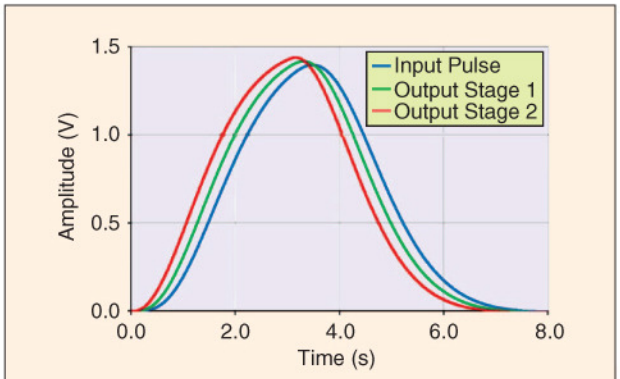

Figure 4. Gaussian pulse input and temporally advanced output.

III. Implementation in Basic Electronic Circuitry

TASD has been demonstrated to occur in electronic circuitry developed by a number of workers [1–6].

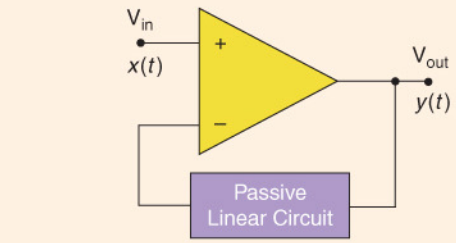

Figure 5. Simplified SA circuit block diagram.

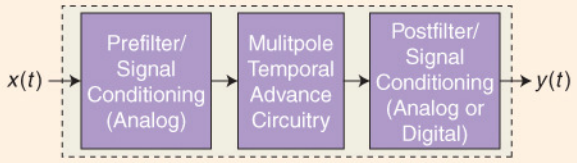

Figure 6. SA circuit with pre- and post-filtering/signal conditioning.

A simplified block diagram of a typical SA circuit is shown in Fig. 5.

The circuit consists of a high gain operational amplifier whose output is fed back to its inverting input (negative feedback) after passing through a passive linear feedback circuit (PLFC). This PLFC consists of a combination of resistive, capacitive, and/or inductive components. A signal applied to a PLFC typically exhibits a temporal delay as the energy from the signal is stored in the electric field of the capacitors and the magnetic field of the inductors while it passes through these circuit components. High-gain op amps function to reduce the difference between the respective signals applied to their inverting (−) and non-inverting (+) inputs.

In this circuit configuration, the output signal from the op amp passes through the feedback circuit incurring a time delay before being applied to the inverting input. This slightly delayed and inverted output recursively (repeatedly) applied to the inverting input results in the leading or foremost portions of the input waveform being differentially amplified, while the lagging portions are attenuated. The number of repeated cycles and the delay in the feedback loop are a function of the op amp response time and the overall impedance of the PLFC. For a given op amp, the values of the components comprising the PLFC in the feedback loop determine the overall signal transforming characteristics of the temporal advance circuitry.

Alternate explanations for how TASD occurs in electronic circuits have been offered by other investigators. For example, "… for operational amplifiers with a sufficiently high gain-feedback product, the voltage difference between the two input signals arriving at the inverting and non-inverting inputs of the amplifier must remain small at all times. The operational amplifier must therefore supply a signal with a *negative* group delay at its output, such that the *positive* delay from the passive filter is exactly canceled out by this negative delay at the inverting input port." [3] and "… there is sufficient information in the early portion of any analytic voltage waveform to reproduce the entire waveform earlier in time" [6]. Empirically, the net result is that "this negative feedback circuit will produce an output pulse whose peak leaves the output port of the circuit *before* the peak of the input pulse arrives at the input port of this circuit" [3].

IV. Pre- and Post Filtering/Conditioning

A functional block diagram of a single SA circuit is shown in Fig. 6. Depending on the specific application, an SA circuit may include the following sub-stages:

1) A pre-filter/signal conditioning stage (analog only),
2) A temporal advance circuit stage (analog), and
3) A post-filter/signal conditioning stage (analog or digital).

It is important to note that the pre-filter/signal conditioning stage consists of analog circuitry (not digital), whereas the post-filter/signal conditioning stage may be implemented using either analog or digital electronics. Recall that temporal advance circuitry functions to selectively amplify the very early, signal perturbations (referred to as forerunners [12]) effectively imparting a temporal advance to the analog signal detection. If the input signal is subjected to digital filtering/signal conditioning prior to its application to the temporal advance circuit, these early, low amplitude perturbations would be lost during the conversion from analog to digital.

Pre-filtering may be used to band limit the incoming signals and, in the case of cascaded SA circuits (discussed below), reduce or eliminate distorting noise from preceding stages. Post-filtering may be used to eliminate distortions resulting from the temporal advance circuit sub-stage. It should also be noted that in order to achieve an overall signal detection temporal advance, any required pre- and/or post-filter stage must operate in less time than the temporal advance achieved by the SA circuit stage. Readily available operational amplifiers [16–18] and digital converters/processors (A2D/DSP/D2A combined) [19–21] that can be used for signal conditioning have response times several orders of magnitude faster than the TASD achievable in lower frequency applications (under 500 Hz).

Table 1.
Input pulse width/frequency and temporal advance.

Study	Pulse Width	Equivalent Frequency	Advance	Percent Advance
Hymel [14]	2.44 s	0.20 Hz	0.9 s	36.9%
Kitano, et al. [4]	1.95 s	0.26 Hz	0.5 s	25.6%
Chaio, et al. [3]	37.5×10^{-3} s	13 Hz	12.1×10^{-3} s	32.3%
Hymel [14]	20.0×10^{-3} s	25 Hz	5.3×10^{-3} s	26.5%
Hymel [14]	5.0×10^{-3} s	100 Hz	1.53×10^{-3} s	30.6%
Zhilu, et al. [8]	1.57×10^{-3} s	320 Hz	0.66×10^{-3} s	42.0%
Hymel [14]	0.67×10^{-3} s	750 Hz	0.31×10^{-3} s	46.5%
Munday, et al. [5]	0.17×10^{-3} s	3000 Hz	0.078×10^{-3} s	46.8%
Erickson, et al. [22]	0.15×10^{-3} s	3300 Hz	0.047×10^{-3} s	31.7%

V. Comparison of Previous Studies

The results of a number of studies investigating TASD over a range of input signal bandwidths reveal a consistent relationship between the primary wavelength/pulse width and the temporal advance that was achieved. For studies in which the input signal was sinusoidal, the period of the signal's highest frequency component (representing the minimum pulse width of the signal) was defined as the pulse width at one half amplitude of a raised cosine with a period equal to the inverse of the frequency of the sinusoid.

Table 1 summarizes these results for inputs with half amplitude pulse widths ranging from about 2 s to 150 μs corresponding to a spectral range of 0.2 Hz to 3.3 kHz. The summary shows the duration of the temporal advance obtained as a percentage of the input pulse width. These results are summarized in Fig. 7. The temporal advance achieved with a single circuit stage relative to the input pulse width ranges from 30 to 40% averaging about 35%. For example, for a bioelectric waveform in which the range of spectral content of interest is less than 100 Hz and the period is 10 ms, the half amplitude pulse width is 5 ms. As such, the signal detection temporal advance expected from a single circuit stage is about 1.5 ms. Similarly, for a circuit designed for signals with spectral content less than 25 Hz, the expected detection temporal advance would be around 5 ms.

VI. SA Circuit Stage Cascading

The signal detection temporal advance that may be achieved in a single circuit stage appears to be limited to a fraction of the narrowest half-cycle pulse width of its input analog signal [1,4,5,23]. Serial cascading of SA circuit stages (Fig. 8) to increase the overall temporal advance has also been demonstrated. It has further been suggested that the resulting advance could exceed the narrowest input pulse width [3,4,23] but is likely limited to a few (perhaps 2 to 4) pulse rise times (about one quarter of the equivalent wave period) [15]. As the temporal advance increases through the cascading of multiple stages, signal distortion tends to increase due possibly to "ringing" – the generation of higher frequency components close to the circuit's resonant frequency. All this suggests that the overall advance obtainable, even with sequential cascading, may be limited to about one full period of the highest frequency component of the signal.

Cao, et al, [23] demonstrated that cascading could increase the temporal advance of the signal within a

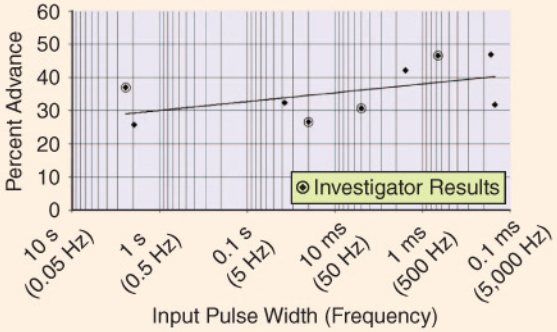

Figure 7. Percent signal advance relative to input pulse width (frequency).

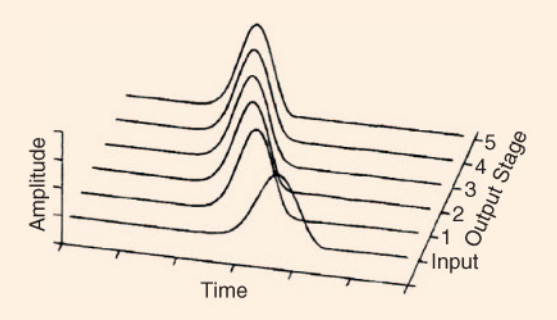

Figure 8. Cascading SA circuits.

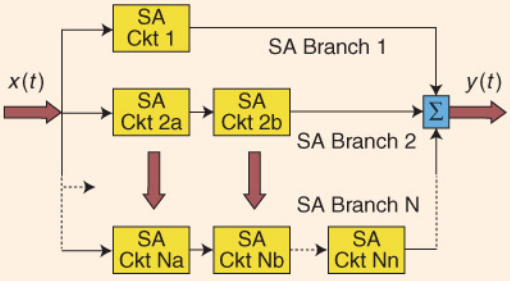

Figure 9. Parallel SA circuit array.

narrow bandwidth with waveform distortion limited to pulse-width compression. This however required highly filtered input waveforms [4,23]. It has been further demonstrated that multi-pole (i.e., having multiple resonances or characteristic frequencies) SA circuitry may be designed that exhibits a relatively constant temporal advance and gain for band-limited signals [5].

VII. Extensions Using Parallel Arrays

Parallel arrays of narrowband SA circuits (where single SA circuits are additionally cascaded) may be configured to generate a more application specific input-output response (Fig. 9). Such a parallel arrangement could provide a mechanism to achieve a temporal signal advance over specific spectral frequency bands tuned to detect certain aspects of the incoming analog signal.

In general, the narrower the spectral band over which the SA circuit operates, the less complicated the SA circuit design. In addition, the lower the maximum frequency the greater the detection temporal advance that can be achieved per stage. Thus fewer cascade stages might be required as the obtainable advance is a function of the highest frequency (narrowest half-cycle pulse width) in the input signal

Parallel configurations using narrowband SA circuits could yield a more linear input/output response in terms of gain and temporal advance over narrow spectral ranges of interest. Further, they could be configured to impart varying delays/advances over certain spectral ranges, effectively acting as spectral filters temporally separating waveform components based on their spectral content. In this configuration, an SA filter band could be employed to differentially advance specific frequency components in order to reveal certain masked signal elements.

VIII. Circuit Modeling and Simulation

The work described above enabled the design of an SA circuit model that exhibits TASD of a band-limited input signal. Our design objectives were to produce a circuit whose transfer function exhibits 1) a constant temporal advance over a pre-specified frequency band; 2) a gain response within $\pm 10\%$ of unity within this frequency band, and 3) minimal shape distortion of the output signal with respect to the input signal. First we developed circuit models for the frequency ranges of 1 to 100 and 1 to 500 Hz. Subsequently, we used these preliminary designs to develop a 1 to 25 Hz model for use in testing the temporal advancement of ECG (heart beat) waveforms.

Anasoft's Super-SPICE Gold Professional Circuit Analysis software package was used to design, simulate and test the models [24]. SPICE was used to numerically simulate the idealized theoretical performance of the circuit model using the software's AC analysis function. This analysis yielded response functions used to compute the circuit model's gain, phase and group delay, each with respect to frequency.

It is important to recognize the difference between the development and testing of a theoretical model and a circuit simulation using SPICE. The theoretical analysis is dependent on mathematical models and assumes idealized component performance, whereas the circuit simulation requires the application of signals to the circuit model taking into account simulated component (manufacturer) performance data. Thus any theoretical results must subsequently be validated through circuit simulation and ultimately, in actual circuitry.

Additionally, the refined circuit design was mathematically modeled in order to have another comparison metric against both the SPICE theoretical and simulated performance results. For the SPICE simulations we replaced the large value inductors with gyrator circuits (large valued inductors cannot be physically realized in microelectronic circuitry). Gyrators use capacitors, resistors and operational amplifiers to simulate large inductive impedances [25,26]. The performance of the circuits modeled and simulated using gyrators instead of inductors was practically identical to the theoretical models using inductors only. Initial efforts involved first replicating and then later improving upon the design of several SA circuits described in the literature [3,4,5].

An SA circuit model that exhibited a fairly constant response over a spectral range of 1 to over 2500 Hz was reported by Munday and Henderson [5]. The main objective of our work was to develop an SA circuit model that produces a relatively constant gain and temporal advance response in the frequency band of 1 to 25 Hz. To achieve this, the initial design work involved changing the circuit component (resistors, capacitors and inductors) values used in the model reported by Munday and Henderson [5] to lower values similar to those used by Mitchell and Chaio [1]. The component values

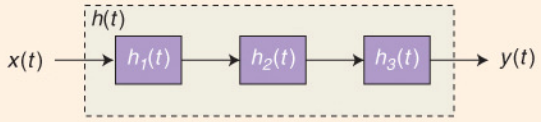

Figure 10. Single stage SA circuit model consisting of three substages.

were adjusted iteratively to obtain the desired response characteristics. They were later replaced with values that match available physical components and accommodate maximum voltage/current values and leakage currents. Further refinements to the design were required for noise suppression and adjusting the output gain.

The refined circuit model incorporates three substages as shown in Fig. 10.

The generalized circuit model transfer function is

$$H(s) = \mathcal{L}\{h(t) = h_1(t) * h_2(t) * h_3(t)\} \rightarrow$$
$$H(s) = [1 + N_1(s)/D_1(s)] \times [1 + N_2(s)/D_2(s)] \times G$$

where s is the complex frequency variable ($s = j\omega$), $\mathcal{L}$ is the Laplace transform operator, $h(t)$ is the overall impulse response of the circuit and * is the convolution operator. The N(s)'s are the resulting complex numerators for the first and second stages, the D(s)'s are their complex denominators and G, the third stage, is a scalar gain multiplier implemented as a resistance voltage divider. In this SA circuit design, the function H(s) has four zeros and four poles (two complex conjugate pairs for each) all located on the left hand side of the s plane indicating circuit stability (Fig. 11). The transient response or settling time of the circuit is about 375 ms.

The design was tested using Gaussian pulses and Gaussian-windowed sinusoids of various types (single and triple frequency signals). Gaussian-windowing (or filtering) was selected since the majority of the previous SA studies employed Gaussian waveforms due to their rapid spectral roll-off and mathematical simplicity [1–4,6,23].

In an early circuit model design, a dual-stage (cascaded) SA circuit board was assembled and tested using a Gaussian pulse with a half amplitude width of about 2 s as input. Fig. 12 is a time-lapsed image of a dual-trace oscilloscope (timescale: 0.5 s/div) showing the temporally advanced output pulse relative to the input. The signal detection advance achieved in each stage was roughly 0.45 s resulting in a 0.9 s overall advance.

Note the low to moderate amount of output distortion (i.e., slightly narrowed pulse width, skewing toward the left and increased peak amplitude) with respect to the input signal. Subsequent work focused on the development of SA circuitry designed to detect and temporally advance the ECG of a human heartbeat.

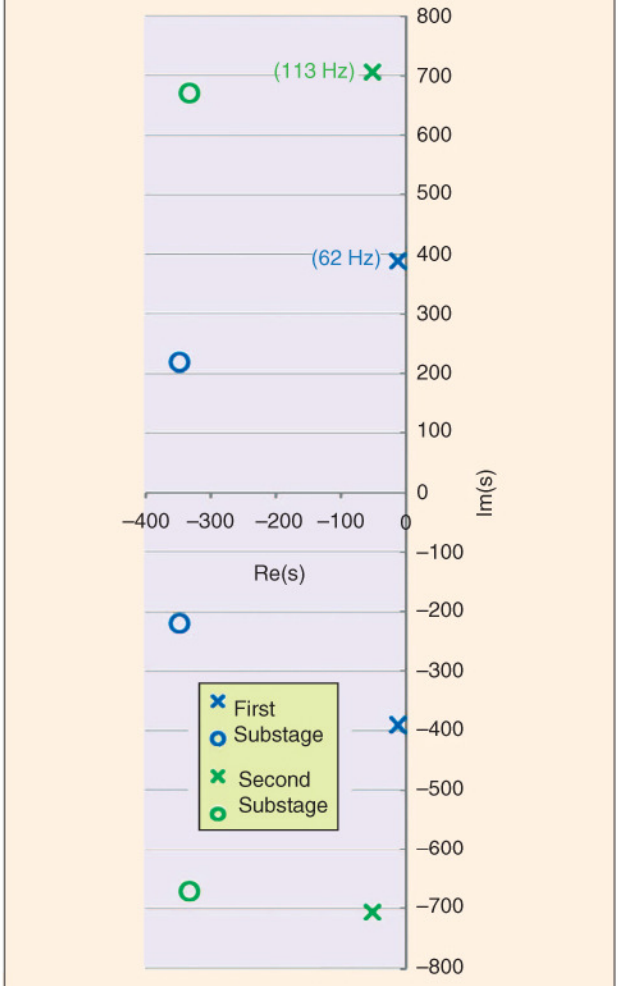

Figure 11. Poles and zeros of the SA circuit transfer function.

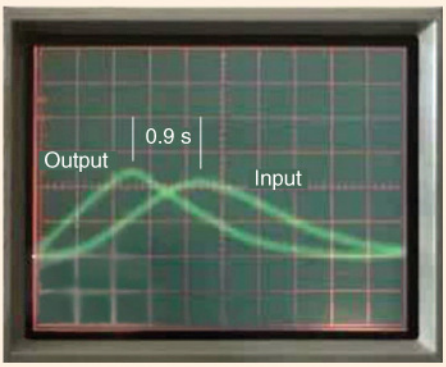

Figure 12. SA circuit output vs. input.

Figs. 13–15 are graphs of the gain, phase and group delay response characteristics respectively of the refined

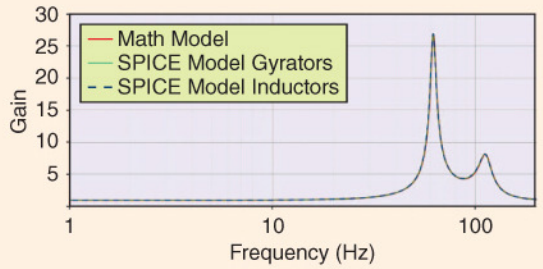

Figure 13. Gain vs. frequency (semi-log plot) for the math, SPICE inductor and SPICE gyrator-based SA circuit models.

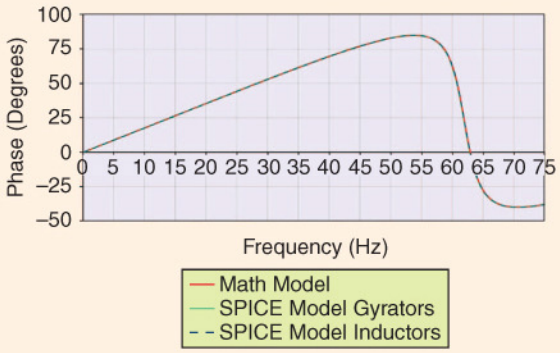

Figure 14. Phase vs. frequency (linear-linear plot) for the math, SPICE inductor and SPICE gyrator-based SA circuit models.

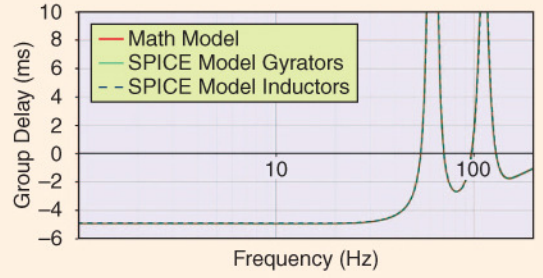

Figure 15. Group delay vs. frequency (semi-log plot) for the math, SPICE inductor and SPICE gyrator-based SA circuit models.

circuit model design (1 to 25 Hz). These figures show results comparing 1) the mathematical model with the SPICE theoretical model having 2) inductors, and 3) gyrators replacing inductors. Note that the three plots in each of Figs. 13–15 overlap each other almost precisely, doubly validating the findings.

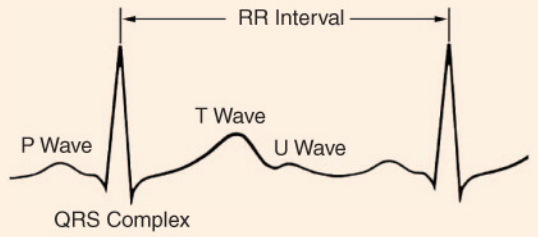

Figure 16. Normal sinus rhythm in the ECG heartbeat pattern.

IX. Application to Constructed Signals and Human ECGs

A. Methods

We tested this circuit model's performance using four types of input signals [13], three of them "constructed," plus human ECGs. The constructed signals consisted of 25 waveforms in each of three groups as follows:

- Gaussian pulses with half amplitude pulse widths ranging from 20 to 500 ms. These pulse widths are equivalent to one half of the periods of 1 to 25 Hz sinusoids,
- Gaussian tapered single frequency sine waves ranging from 1 to 25 Hz, and
- Gaussian tapered triple frequency sinusoids. To construct each of these input signals, an integer frequency was randomly selected from each of the following ranges: 1 to 8 Hz, 9 to 16 Hz, and 17 to 25 Hz. In addition, each of the three spectral components was scaled by one of three randomly selected gain factors (0.2, 0.3 and 0.45) in order to ensure that their linear combination did not exceed the maximum amplitude threshold in the event that the amplitude peaks or troughs were coincident.

A number of signal characteristics make the ECG an ideal candidate for the investigation of SA technology (Fig. 16):

- The ECG is generally a well-defined waveform containing "signature" voltage deflections designated P, Q, R, S, T, U with specific time intervals between the deflections.
- The QRS complex has a high signal-to-noise ratio (SNR).
- ECG signal amplitudes are measured in millivolts (vs. microvolts for EEG signals).
- A number of cardiac pathologies are reflected not only by changes in ECG voltage deflections but in deviations from normal of the various time intervals.

Twenty single ECG heartbeats from five human subjects were selected for testing (100 ECG waveforms in total). Three of the subjects exhibited normal sinus rhythm and two subjects exhibited tachycardia (rapid heart rate). Each heartbeat signal was Gaussian tapered similarly to the single and triple frequency constructed signals to reduce any high frequency ringing artifacts at the beginning and end points of each signal.

Of the five sets of unfiltered ECG recordings, used as input signals, two of the subject's ECG data were recorded with a sampling rate of 1000/s [27] and three [28] were recorded at 200/s. The ECG waveforms were "raw" – they were purposely not subjected to lowpass filtering when acquired in order to study the circuit's distorting effects on frequencies beyond the high pass cutoff of the circuit design (25 Hz). The (input) ECG signals were subsequently upsampled to 20,000/s. This rate far exceeds the Nyquist criterion [29] thus allowing sufficiently fine measurement of temporal intervals. Finally, cubic spline interpolation was applied to all the signals, effectively upsampling them ten more times (to a rate of 200,000/s), in order to provide an even more precise estimate of results. This increased the *apparent* resolution of the data without adding any new information [30].

Fig. 17 shows an example of results obtained when the ECG from a single human heartbeat was applied to a one-stage SA circuit. We see the clear result that the output waveform of the circuit (red) leads its input (by slightly under 5 ms) with very little distortion.

To determine the temporal advance for each test signal, the cross-correlation function between the input and output signals was computed so as to determine the "lead" value that corresponds to the cross-correlation maximum. This function determines the linear relationship between two waveforms as one of them is shifted in time relative to the other [31].

The circuit gain was determined by calculating the Root Mean Square (RMS) ratio of the temporally advanced signal output relative to the input. The mean (μ), standard deviation (σ) and coefficient of variation ($C_v = \sigma/\mu$) were computed for each type and group of signals studied. In addition to these time domain measures, extensive Fourier analysis was performed as a cross check against the time domain results (these results are not specifically reported here).

B. Temporal Advance and Gain Results

Fig. 18 shows the overall temporal advance results of the simulations for the three groups of constructed input signals (Gaussian pulses, single frequency and triple frequency sinusoids) and for each of the five subject's ECGs. Each bar represents the mean temporal advance in its respective group with error bars representing σ.

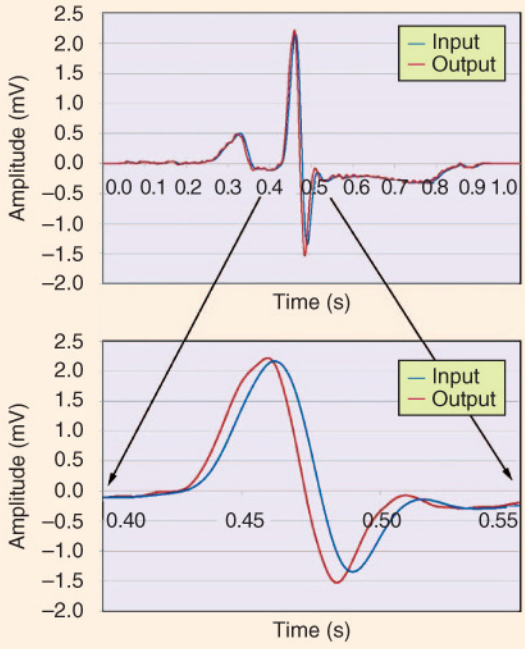

Figure 17. Temporally advanced detection of a human heartbeat.

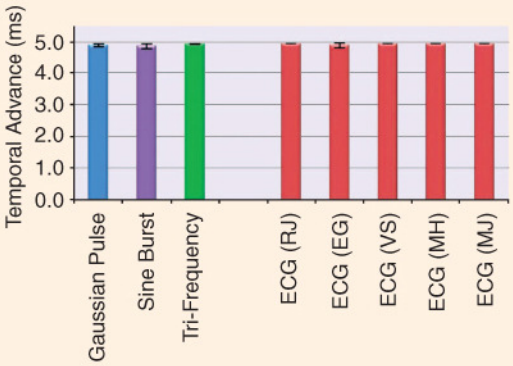

Figure 18. Overall temporal advance results.

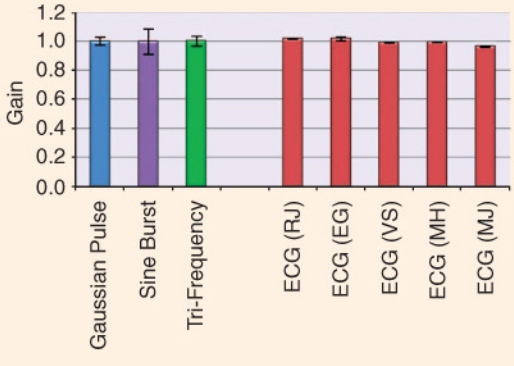

Figure 19. Overall gain results.

The results are consistent across the board: the overall mean temporal advance was 4.93 ms with a C_v of less than 1%.

Fig. 19 shows the results of the gain analyses. Again, the results across the board are highly consistent with very low variance. The overall mean gain is 0.997 with a C_v of less than 0.5%.

C. Distortion Ratio

In the majority of the cited TASD studies, temporally advanced output waveforms exhibit significant waveform distortions observed in the frequency domain. This was examined in detail with the circuit model. Fig. 12 above shows an example of the distortion in output signal waveshape in the initial physical circuit. In the frequency domain, pulse narrowing results in a phase shift to a higher frequency and the skewing of the pulse results in the introduction of higher frequency components in the output waveform that are not present in the input waveform. Given the constancy of both the gain and group delay in the spectral range of interest for the SA circuit model under investigation, these types of distortion were not expected to be present and in fact were not evident based on visual inspections of the input/output spectral distributions.

The distortion ratio (DR) [32] may be determined most easily in the frequency domain by 1) subtracting the spectral magnitude of the input from the corresponding spectral magnitude of the advanced output at each frequency, 2) the differences are squared and then summed over all the frequencies of interest, 3) the result is then divided by the sum of the squares of the input signal magnitude over all frequencies, and 4) finally, the square root of the result is taken, giving a root mean square ratio. In equation form,

$$\mathrm{DR} = \left[\sum_f (\mathrm{Y}(f) - \mathrm{X}(f))^2 / \sum_f \mathrm{X}(f)^2\right]^{1/2},$$

where the summations are over the frequency range of interest. DRs were computed for the triple frequency signals and for all ECGs. The overall DR results are summarized in Fig. 20. The mean DR is less than 8% over all the test signals. For the ECGs, the DR over the frequency range of 0.5 to 25 Hz is less than 6%.

The ECG results suggest that the majority of the overall distortion occurs in the spectral range of 0.5 to 25 Hz. The ECG test signals used in this study had not been (pre)filtered, thus they contain frequencies above 25 Hz. In clinical practice, this spectral content would normally be reduced or eliminated through first filtering the acquired ECGs. The input signals were spectrum analyzed to determine the relative distribution of frequency content above and below 25 Hz. The average results over all of the subjects showed that spectral content below 25 Hz accounted for over 93% of the total amount, while less than 7% comes from spectral content above 25 Hz (up to approximately 200 Hz).

D. Waveform Dissimilarity

Correlation may be used as a measure of the morphological similarity between two waveforms [33,34]. Additionally, as stated by Semmlow [35], "in correlation, the coefficients are normalized to fall between zero and one. This makes the correlation coefficients insensitive to variations in the gain … or of the scaling of the variables." Based on the use of correlation coefficients as a measure of waveform similarity, its complement, dissimilarity, is naturally defined as the difference between perfect correlation (1.0) and that between the input and its respective output magnitude spectra. It therefore provides a relative measure of the morphological *dissimilarity* between the waveforms that is unaffected by the gain variation [35,36]. The overall mean input/output waveform dissimilarity was determined to be less than 0.3% (Fig. 21).

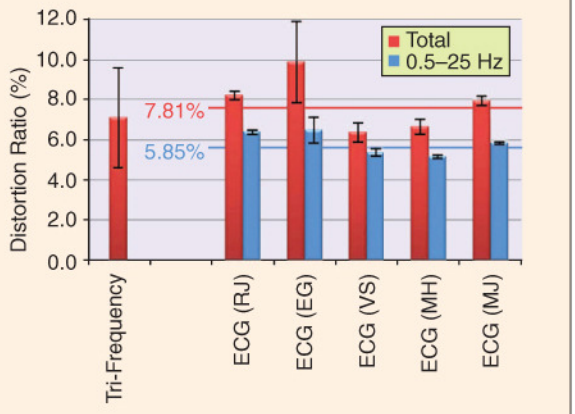

Figure 20. Input/output distortion ratios.

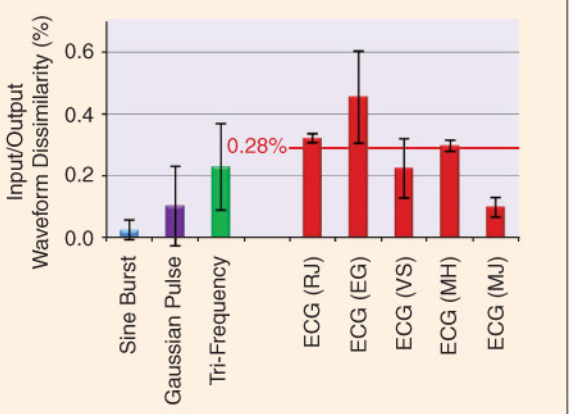

Figure 21. Input/output waveform dissimilarity.

X. Potential Applications of SA Technology

In general, an SA circuit acts to offset analog signal detection and processing delays thereby decreasing the overall system response time. As such, ideal applications are those in which a faster response time will improve performance. These applications would typically be closed-loop control or interventional type systems. Simple monitoring applications however, may not derive significant benefit from faster overall signal detection/processing. As shown in Fig. 7, it is clear that there is an indirect relationship between a signal's frequency and the duration of the temporal advance that may be achieved using a single SA circuit stage. As such, applications in which the analog signals change more slowly may facilitate implementation of SA technology.

In general, SA technology could be applied to temporally advance 1) narrowband signals to offset delays associated with filtering, and/or 2) broadband signals (offsetting overall signal processing delays). In addition, differential SA technology using multiple spectrally tuned bands of SA circuits might be used to temporally separate overlapping signal components facilitating masked signal component separation/detection in a host of responsive systems. It has potential applications in a broad range of signal detection and processing systems, both biomedical and non-biomedical.

A. Biomedical

SA technology may be well suited for medical instruments and treatment devices as well as electrophysiological interfaces used in the detection, acquisition and processing of band-limited analog waveforms produced by the body (e.g., brainwaves such as the EEG and MEG; neuromuscular potentials – EMG (electromyogram); cardiac rhythms – ECG). The ability to provide faster, more immediate detection of and a more rapid response to anomalous signals or alarm conditions may enable more effective control or intervention.

Regarding real-time applications, TASD may offset signal processing delays associated with the extraction of relevant features thereby improving response times and overall system performance. Additionally, SA technology using multiple spectrally tuned bands of single-stage SA circuits in parallel (see Fig. 9) has the potential to temporally shift overlapping signal components (artifacts/noise) differentially to allow unmasking of bioelectric signal components of interest, which in turn might facilitate artifact detection/correction. The ability to temporally separate anomalous or artifactual signal components based on their spectral content may facilitate earlier detection/intervention.

Some potential biomedical applications include real-time artifact detection/correction, neural pacing/seizure suppression, neurofeedback/neurotherapy, brain-computer/neural interfaces, and electrocardiology. Additionally, SA technology could enhance the performance of physiologically gated diagnostic and therapeutic applications (such as medical imaging and radiotherapy) by temporally advancing the detection of certain trigger signals thereby improving target and timing accuracy.

Various sources of artifacts often lead to unwanted signal components that overlap or mask the electrophysiological signals of interest. Much of the current artifact detection/correction research focus is on reducing the computational load of present artifact-rejection algorithms in order to reduce their processing time [37–39]. A number of these techniques operate in the frequency domain over narrow spectral bands.

In electrocardiology, waveform components indicative of fibrillation (F-waves) or tachyarrhythmia are typically masked by the large amplitude ventricular QRST complex [40,41]. Furthermore, the ability to rapidly distinguish life-threatening ventricular fibrillation from arrhythmias is critical for avoiding lethal consequences given the short time available to intervene [42,43]. The performance features most critical to successful seizure suppression and neural pacing include high sensitivity and specificity as well as rapid or early detection. Earlier detection of epileptiform EEG signals and faster overall response should improve intervention efficacy [44,45].

In gated imaging and radiotherapy, movement due to either respiration or cardiac activity has a negative effect on diagnosis and treatment, respectively. In the case of imaging this is reflected in either poor image quality or the need for additional scans (which is difficult on patients) [46,47]. With radiation therapy, movement due to respiratory or cardiac activity may lead to unintended irradiation of normal tissue and/or decreased radiation of the targeted cancerous tissue [48,49].

For each of these applications, reducing response times and/or temporally separating overlapping signals could yield significant improvements in overall system performance. This may allow for more effective treatment of certain conditions, potentially opening the door to a whole new class of medical devices that respond faster than any that is currently available.

For any potential application, the signal characteristics of interest and the application requirements determine the SA circuit design-performance criteria. For example, in the case of ECG used in implantable cardioverter/defibrillators (ICDs), the frequency range of interest is between approximately 10 and 40 Hz (the wave shape is also important regarding the feature extraction characteristics) [50]. Thus the SA circuit would be designed to provide a constant advance and gain

beyond 40 Hz. Contrast this (ICD) application with ECG-gated imaging or radiation therapy in which the only requirement is the detection of the QRS peak. As such, the wave shape is not nearly as important. Some amount of signal distortion may be acceptable in order to increase the peak detection temporal advance.

Respiration rates are typically well under 60 breaths per minute (frequency rate: 1 Hz). Motion of the lungs or other organs resulting from respiration would present a similar movement profile as that of the respiratory cycle. To temporally advance respiratory related signals, SA circuitry can be readily developed that would temporally advance signal detection by over 0.5 s. In respiratory gated radiation therapy, SA circuitry designed for such lower cycle rates could provide a much earlier trigger to terminate tissue irradiation helping to minimize damage to normal tissue and improve target accuracy.

In studies involving the scalp-recorded EEG, the frequency range of interest is under 70 Hz, whereas some electrocorticographic (ECoG) recording studies (using electrodes placed directly on the surface of the brain) indicate activity of interest up to 200 Hz [51,52]. Thus, even for ECoG applications, an SA circuit would need to be designed accordingly, with higher frequency requirements imposing greater single stage and overall cascaded detection temporal advance limitations.

The computational demands of signal interpretation and processing associated with neural interfaces for prosthetic and/or robotic applications still limit cybernetic performance, in which "large time delays are associated with (control) feedback loops" [53]. The steps involved in detecting, processing and interpreting neural signals [54] result in overall response delays in "smart" prosthetic limbs that are much longer than biological response times.

In neurofeedback therapy, EEG signals are acquired and fed back to the subject as a form of operant conditioning [55]. Reducing the amount of feedback delay should improve the efficacy and efficiency of neurotherapy in general [56,57]. A number of neurofeedback systems operate on EEG signals with spectral content from the delta (0.5 to 3.5 Hz) up to the beta range (13 to 30 Hz) [55], others through the gamma range and higher (up to about 100 Hz) [58]. For an application limited to the beta range, an SA circuit design similar to that described earlier in this article might suffice.

In essence, SA circuitry must be designed for each specific application and there will be trade-offs between the temporal advance that may be achieved, the minimum spectral range required, and the tolerable amount of signal distortion. For SA technology to be of practical use in electrophysiological applications, the overall temporal advance achieved must provide a significant offset to the signal processing delay or provide a usable temporal shift for separating masked or overlapping signal components based on spectral content. For near-term applications, the temporally advanced output signal should be a high fidelity representation of the input signal in order to take advantage of current detection, feature extraction and other signal processing methodologies.

B. Non-Biomedical

There are potentially hundred of applications of SA technology involving various types of sensors that operate in a frequency range up to a few thousand Hz. Table 2 shows the categories to which SA technology more than likely applies.

Potential non-biomedical applications/markets include a broad range of commercial, industrial, military and transportation areas such as 1) industrial process control, 2) alarm/detection systems, 3) vehicular/flight control, 4) chemical processing systems, 5) manufacturing/production and 6) military targeting/weaponry.

In industrial process control, a number of physical parameters such as temperature, pressure, flow, etc. are closely monitored and provide input data for closed loop computer control systems that optimize production yields [59,60]. In refining, for example in distillation, "… faster closed loop response (i.e., a shorter natural period) … provides better disturbance rejection" [61]. The transient response times are measured in minutes [62,63], making these processes good candidates for the application of SA technology in order to improve process control response times. The resulting

Table 2.
Categories to which SA technology more than likely applies.

Acoustic/Sound/Vibration	Angle/Rotation	Chemical
Distance/Displacement	Electrical/Electromagnetic	Environment/Weather
Flow	Level/Density	Magnetic/Radio
Navigation	Optical/Light/Imaging	Photoelectric Sensors
Position/Pressure/Force	Proximity/Presence	Radiation/Subatomic Particles
Speed/Acceleration	Thermal/Temperature/Heat	Transportation

improvements in product yields and energy savings as well as safety could translate into millions of dollars in economic benefit.

Compressors run most efficiently when operating near their stability limits. Such conditions require very fast control response times in order to "... suppress rotating stall and surge, ... (and) extend the stable operating range of the compressor ... using feedback control" [64]. To optimize performance and ensure safe operation, compressor control systems rely on real-time pressure, temperature and flow measurement to determine the compressor operating point and surge margin [65]. Overall feedback response delays negatively affect performance [66]. Reducing or eliminating control delays using time-optimal control strategies significantly reduces the probability of compressor stalls and/or surges occurring, thereby enhancing operational stability margins and increasing productivity as well as safety [67,68].

In the area of transportation systems, use of TASD could improve crash avoidance, safety/security, drivetrain performance and overall vehicular control (e.g., hybrid and hydrogen fuel cell performance). For example, in high performance aircraft engine control systems, real-time detection of inlet airflow distortion is used for high speed engine control in order to increase engine stability, reduce stall margin requirements, increase overall performance, and lower fuel consumption [69].

With gas turbine engines, improved flow control performance could "delay separation, enhance mixing of fluids, create 'virtual' shapes, modify wake behavior and reduce drag" [70]. Improvements in flow control include faster closed-loop fuel flow control, compressor operation closer to its stall boundary, fuel/air mixing control and air cooling based on turbine temperature - all areas in which TASD could significantly reduce system response times and improve performance.

This discussion has provided just a few examples of non-biomedical applications that may benefit significantly from use of SA technology. The improvements would most likely be in operating efficiencies (cost reductions), performance/yield and accident prevention/reduction.

XI. Summary and Conclusions

The following has been demonstrated with respect to SA circuit technology:

- The phenomenon of TASD is implementable in electronic circuitry in which the output signal is temporally advanced with respect to the complete detection/acquisition of the circuit input signal.
- TASD relates to what some researchers refer to as superluminal wave propagation. Only portions of the waveform (in particular the detectable group envelope and never the wave front itself) propagate faster than light speed. As a result, TASD and systems that implement it do not violate causality.
- SA circuitry can be designed such that the temporal advance and signal gain are constant over a specified frequency band (e.g., 0.5 to 25 Hz) with minimal waveform distortion.
- Both narrowband and wideband analog waveforms (those with multiple spectral components) can be temporally advanced by SA circuitry.
- SA circuit components are, in general, scalable to accommodate specific input signal spectral ranges.
- Based on previous studies, the signal detection temporal advance that may be achieved is directly related to the input signal pulse width and inversely related to the maximum frequency of the signal.
- The response time of current analog and digital electronics is significantly less than the projected signal detection temporal advance that is likely to be attained.

In conclusion, there appears to be ample evidence that electronic circuitry can be designed that yields both nearly constant amplitude gain and TASD for a wide variety of biomedical as well as non-biomedical signal types. Furthermore, based on direct experimentation and results obtained by a number of investigators, the magnitude of the temporal advance can be increased by cascading multiple SA circuit stages, provided that signal distortion and any introduced artifacts (particularly high frequency oscillations) are kept to a minimum through appropriate and judicious use of filtering and signal conditioning.

Chris M. Hymel is an experienced entrepreneur and scientific/engineering consultant. He has worked in the areas of industrial/process control, computer networking, data acquisition, signal generation and biomedical (neurophysiology) systems for large corporations and universities and as an independent consultant. In addition, Dr. Hymel also ran a medical/legal consultation firm providing personal injury and medical malpractice litigation support as well as accident reconstruction. Dr. Hymel received his B.S. and M.S. in electrical engineering from Texas A&M University and his Ph.D. in biomedical sciences from the University of Texas Health Science Center at Houston. Dr. Hymel holds patents in multiple areas and has authored a

number of scientific articles. His research interests are in the application of emerging technologies to biomedicine. Recent activity has focused on the development of application-specific temporally advanced detection of bioelectric signals to reduce closed-loop delays and improve the overall performance of control/interventional systems.

Malcolm H. Skolnick received his Ph.D. in physics from Cornell University and JD from the University of Houston Law Center. He has recently retired as the President and CEO of a public biotechnology firm. Prior to his service in industry, Dr. Skolnick held academic positions in the Medical School, the Graduate School of Biomedical Sciences and the School of Public Health of the University of Texas Health Science Center at Houston. Prior to joining the School of Public Health, Dr. Skolnick managed the Health Science Center's Office of Technology Management, overseeing the University's activities in protecting and licensing its technology portfolio. He also headed the Neurophysiology Research Center and served as principal investigator of several clinical trials in pain management, smoking cessation and reduction of withdrawal symptoms in drug addiction. Dr. Skolnick is a registered patent attorney, patented inventor and is licensed to practice in Texas. He has been active in patent prosecution and licensing for selected clients and has served as an expert witness in intellectual property, product liability, and accident reconstruction matters. He serves on the Board of Directors of the Southwest Health Technology Foundation.

Ron A. Stubbers has been developing and manufacturing electronic biomedical devices for over 18 years ranging from neurostimulation systems to 512 channel EEG systems. He has also created and managed product design and manufacturing in the areas of engineering, quality, regulatory, technical support, and materials for various start-up companies. A former manager of quality and regulatory affairs, Mr. Stubbers has experience in corporate ISO/EN/QSR systems requirements and compliance, and in European CE and FDA 510K Class II and other regulatory approvals for world-wide medical device distribution. Mr. Stubbers received his BSEE from the University of Idaho and performed graduate work at the University of Texas Health Science Center - Houston and at Rice University.

Michael E. Brandt received his B.S. in physics from the Polytechnic Institute of NYU and the M.S. and Ph.D. in

biomedical engineering from the University of Houston. He was a tenured faculty member of the University of Texas Health Science Center at Houston where he directed the Neurosignal Analysis Laboratory from 1989 to 2009. He led major research projects in cognitive psychophysiology, EEG and evoked potentials, brain-behavior development, neuroimaging, cardiology and immunology. Dr. Brandt has also been involved in a number of nonlinear/chaotic biosystem studies and developed a method based on time-delay feedback to regularize certain clinically aberrant events (e.g., cardiac and seizures). Dr. Brandt has published over 100 peer-reviewed articles, conference proceedings papers and book chapters and has made numerous presentations during his career. He is a Senior Member of the IEEE and is currently an independent technical consultant in the biomedical and energy arenas. His current R&D focus is on biomedical and other applications of signal advance technology.

References

[1] M. W. Mitchell and R. Y. Chiao, "Causality and negative group delays in a simple bandpass amplifier," *Am. J. Phys.*, vol. 66, pp. 14–19, 1998.

[2] J. C. Garrison, M. W. Mitchell, R. Y. Chiao, and E. L. Bolda, "Superluminal signals: Causal loop paradoxes revisited," *Phys. Lett. A*, vol. 245, pp. 19–25, 1998.

[3] R. Y. Chiao, J. M. Hickmann, and D. Solli, "Faster-than-light effects and negative group delays in optics and electronics, and their applications," *Proc. SPIE,* vol. 4283, 2001.

[4] M. Kitano, T. Nakanishi, and K. Sugiyama, "Negative group delay and superluminal propagation: An electronic circuit approach," *IEEE J. Select. Topics Quantum Electron.*, vol. 9, pp. 43–51, 2003.

[5] J. N. Munday and R. H. Henderson, "Superluminal time advance of a complex audio signal," *Appl. Phys. Lett.,* vol. 85, no. 3, pp. 503–505, 2004.

[6] D. Solli and R. Y. Chiao, "Superluminal effects and negative group delays in electronics, and their applications," *Phys. Rev. E,* vol. 5, 2002.

[7] W. Withayachumnankul, B. M. Fischer, B. Ferguson, B. R. Davis, and D. Abbott, "A systemized view of superluminal wave propagation," *Proc. IEEE*, vol. 98, pp. 1–12, 2010.

[8] Z. Zhilu, Y. Zhendong, R. Gaunghui, and Z. Zhonghao, "A novel method of speeding up the signal processing system," in *Proc. ICSP,* 2006, pp.16–20.

[9] H. Noto, K. Yamauchi, M. Nakayama, and Y. Isota, "Negative group delay circuit for feed-forward amplifier," in *IEEE/MTT-S Dig.*, 2007, pp. 1103–1108.

[10] B. Ravelo, A. Perennec, and M. Le Roy, "Synthesis of broadband negative group delay active circuits," in *IEEE MTT-S Dig.,* 2007, pp. 2177–2180.

[11] B. J. Arntz, "Method and apparatus for imparting positive phase slope to a narrow-band signal," U.S. Patent 5 291 156, 1995.

[12] L. Brillouin, *Wave Propagation and Group Velocity (Pure and Applied Physics).* New York: Academic, 1960.

[13] P. White, "Group delay explanations and applications," Applied Radio Labs, Design File DN004, Nov. 1999.

[14] C. M. Hymel, "Application of signal advance technology to electrophysiology," dissertation, Univ. Texas Health Science Center at Houston, Graduate School of Biomedical Sciences, Aug. 2010.

[15] K. T. McDonald, "Negative group velocity," *Am. J. Phys.,* vol. 69, no. 5, pp. 607–614, 2001.

[16] "LM6165/LM6265/LM6365 high speed operational amplifier," National Semiconductor, Literature No. DS009i52, May 1999.

[17] "MAX477 300MHz high-speed op amp," Maxum Integrated Products, Literature No. 9-0467, Rev. 3, Nov. 1999.

[18] "ADA4817-1/ADA4817-2 low Noise, 1 GHz fast FET op amps," Analog Devices, Literature ADA4817-1/ADA4817, Rev. A, Mar. 2009.

[19] "ADS1605 24-Bit wide bandwidth analog-to-digital converter," Texas Instruments, Literature No: SBAS274, Mar. 2003.

[20] "TMS320VC5509A fixed-point digital signal processor—Data manual," Texas Instruments, Literature No: SPRS205E (Revised), Aug. 2005.
[21] "56F8023 data sheet (preliminary technical data) 56F8000—16-Bit digital signal controllers," Freescale Semiconductor, MC56F8023, Rev. 3, Mar. 2007.
[22] S. J. Erickson, M. Khaja, and M. Mojahedi, "Time- and frequency-domain measurements for an active negative group delay circuit," *IEEE Antennas Propagat. Mag.*, vol. 3A, pp. 790–793, 2005.
[23] H. Cao, A. Dogariu, and L. J. Wang, "Negative group delay and pulse compression in superluminal pulse propagation," *IEEE J. Select. Topics Quantum Electron.,* vol. 9, pp. 52–58, 2003.
[24] K. Aylward. (2009). Super-SPICE gold professional circuit analysis package [Online]. Available: http://www.anasoft.co.uk
[25] P. Horowitz and W. Hill, *The Art of Electronics*. New York: Cambridge Univ. Press, 1998, pp. 266–281.
[26] R. Schaumann and M. E. Van Valkenburg, *Design of Analog Filters*. New York: Oxford Library Press, 2001.
[27] Electrogram Libraries, ECG Traces: AAEL203, AAEL 204, Chicago, IL, 2009.
[28] H.-T. Shih, Center for Cardiac Arrhythmias, Houston, TX, 2009.
[29] W. Kester. (2009). What the Nyquist criterion means to your sampled data system design. *Analog Dev.* [Online]. Available: http://www.analog.com/static/imported-files/tutorials/MT-002.pdf
[30] S. McKinley and M. Levine. Cubic Spline interpolation [Online]. Available: http://online.redwoods.cc.ca.us/instruct/darnold/laproj/Fall98/SkyMeg/Proj.PDF
[31] J. S. Bendat and A. G. Piersol, *Random Data: Analysis and Measurement Procedures*. New York: Wiley Intersciences, 1971.
[32] A. Baggini, *Handbook of Power Quality*. New York: Wiley, 2008.
[33] E. P. Gerstenfeld, S. Dixit, D. J. Callans, Y. Rajawat, R. Rho, and F. E. Marchlinski, "Quantitative comparison of spontaneous and paced 12-lead electrocardiogram during right ventricular outflow tract ventricular tachycardia," *J. Am. Coll. Cardiol.,* vol. 41, pp. 2046–2053, 2003.
[34] D. Tihelka and J. Romportl, "Exploring automatic similarity measures for unit selection tuning," in *Proc. 10th Ann. Conf. ISCA*, Brighton, Great Britain, 2009, pp. 736–739.
[35] J. L. Semmlow, *Biosignal and Biomedical Image Processing: MATLAB-Based Applications,* vol. 1. Boca Raton, FL: CRC Press, 2004.
[36] R. D. Throne, J. M. Jenkins, and A. L. DiCarlo, "Intraventricular electrogram analysis for ventricular tachycardia detection: Statistical validation," *Pacing Clin. Electrophysiol.*, vol. 13 (part 1), pp. 1596–1601, 1990.
[37] S. Choi, A. Cichocki, H.-M. Park, and S.-Y. Lee, "Blind source separation and independent component analysis: A review," *Neural Inf. Process Lett. Rev.*, vol. 6, pp. 1–57, 2005.
[38] A. Delorme, T. Sejnowski, and S. Makeig, "Enhanced detection of artifacts in EEG data using higher-order statistics and independent component analysis," *NeuroImage,* vol. 34, pp. 1443–1449, 2007.
[39] S. Halder, M. Bensch, J. Mellinger, M. Bogdan, A. Kübler, N. Birbaumer, and W. Rosenstiel, "Online artifact removal for brain-computer interfaces using support vector machines and blind source separation," in *Computational Intelligence and Neuroscience*. Hindawi, 2007.
[40] J. Brazdzionyte, I. Bluzaite, J. Bluzhas, and A. Mickeviciene, "Dynamics of the data of signal-averaged electrocardiogram and their relation to ventricular rhythm disturbancies in myocardial infarction," *J. Hong Kong Coll. Cardiol.,* vol. 4, pp. 72–76, 1996.
[41] M. Stridh and L. Sörnmo, "Shape characterization of atrial fibrillation using time-frequency analysis," *Comput. Cardiol.*, vol. 29, pp. 17–20, 2002.
[42] I. Jekova, "Estimation of electrocardiogram peak frequency and periodicity during ventricular fibrillation," *Comput. Cardiol.,* vol. 30, pp. 225–228, 2003.
[43] M. Haïssaguerre, N. Derval, F. Sacher, L. Jesel, I. Deisenhofer, L. de Roy, J.-L. Pasquié, A. Nogami, D. Babuty, S. Yli-Mayry, C. De Chillou, P. Scanu, P. Mabo, S. Matsuo, V. Probst, S. Le Scouarnec, P. Defaye, J. Schlaepfer, T. Rostock, D. Lacroix, D. Lamaison, T. Lavergne, Y. Aizawa, A. Englund, F. Anselme, M. O'Neill, M. Hocini, K. T. Lim, S. Knecht, G. D. Veenhuyzen, P. Bordachar, M. Chauvin, P. Jais, G. Coureau, G. Chene, G. J. Klein, and J. Clémenty, "Sudden cardiac arrest associated with early repolarization," *New Engl. J. Med.,* vol. 358, pp. 2016–2023, 2008.
[44] I. Osorio, M. G. Frei, B. F. Manly, S. Sunderam, N. C. Bhavaraju, and S. B. Wilkinson, "An introduction to contingent (closed-loop) brain electrical stimulation for seizure blockage, to ultra-short-term clinical trials, and to multi-dimensional statistical analysis of therapeutic efficacy," *J. Clin. Neurophysiol.*, vol. 18, pp. 533–544, 2001.
[45] A. B. Gardner, A. Krieger, G. Vachtsevanos, and B. Litt, "One-class novelty detection for seizure analysis from intracranial EEG," *J. Mach. Learn. Res.,* vol. 7, pp. 1025–1044, 2006.
[46] B. Desjardins and E. A. Kazerooni, "ECG-gated cardiac CT," *Am. J. Roentgenol.,* vol. 182, pp. 993–1010, 2004.
[47] H. D. Park, S. P. Cho, and K. J. Lee, "A method for generating MRI cardiac and respiratory gating pulse simultaneously based on adaptive real-time digital filters," *Comput. Cardiol.,* vol. 33, pp. 813–816, 2006.
[48] S. B. Jiang, "Technical aspects of image-guided respiration-gated radiation therapy," *Med. Dosim.*, vol. 31, pp.141–151, 2006.
[49] S. Webb, "Motion effects in (intensity modulated) radiation therapy: A review," *Phys. Med. Biol.*, vol. 51, pp. R403–R425, 2006.
[50] J. Gillberg, "Detection of cardiac tachyarrhythmias in implantable devices," *J. Electrocardiol.*, vol. 40, pp. S123–S128, 2007.
[51] E. C. Leuthardt, G. Schalk, J. R. Wolpaw, J. G. Ojemann, and D. W. Moran, "A brain–computer interface using electrocorticographic signals in humans," *J. Neur. Eng.,* vol. 1, pp. 63–71, 2004.
[52] A. Schwartz, X. Cui, D. Weber, and D. Moran, "Brain-controlled interfaces: Movement restoration with neural prosthetics," *Neuron*, vol. 52, pp. 205–220, 2006.
[53] M. Kawato, "Brain controlled robots," *HFSP J.,* vol. 2, pp. 136–142, 2008.
[54] M. Van Gerven, J. Farquhar, R. Schaefer, R. Vlek, J. Geuze, A. Nijholt, N. Ramsey, P. Haselager, L. Vuurpijl, S. Gielen, and P. Desain, "The brain-computer interface cycle," *J. Neur. Eng.,* vol. 6, pp. 041001, 2009.
[55] H. Heinrich, H. Gevensleben, and U. Strehl, "Annotation: Neurofeedback—train your brain to train behaviour," *J. Child Psychol. Psyc.,* vol. 48, pp. 3–16, 2007.
[56] W. T. Maddox, F. G. Ashby, and C. J. Bohil, "Delayed feedback effects on rule-based and information-integration category learning," *J. Exp. Psychol. Learn.,* vol. 29, pp. 650–662, 2003.
[57] D. A. Williamson and E. B. Blanchard, "Effect of feedback delay upon learned heart rate control," *Psychophysiology*, vol. 16, pp. 108–115, 2007.
[58] T. R. Schneider, S. Debener, R. Oostenveld, and A. K. Engel, "Enhanced EEG gamma-band activity reflects multi-sensory semantic matching in visual-to-auditory object priming," *NeuroImage*, vol. 42, pp. 1244–1254, 2008.
[59] M. Andersson, Furusjö, and Å. Jansson, "Production optimisation in the petrochemical industry by hierarchical multivariate modelling," IVL Swedish Environmental Research Institute Ltd., Report B1586-A, June 2004.
[60] N. Kasuan, Z. Yusuf, M. N. Taib, M. Hezri, F. Rahiman, N. Tajuddin, M. Azri, and A. Aziz, "Robust steam temperature regulation for distillation of essential oil extraction process using hybrid fuzzy-PD plus PID Controller," *World Acad. Sci. Eng. Technol.,* vol. 71, pp. 932–937, 2010.
[61] P. S. Fruehauf and D. P. Mahoney, "Distillation column control design using steady state models: Usefulness and limitations," *ISA Trans.,* vol. 32, pp. 157–175, 1993.
[62] R. C. Darton, Ed., *Distillation and Absorption* (IChemE Symposium Series Nr 142, vols 1 and 2). Rugby: IChemE, 1997.
[63] S. Skogestad and M. Morari, "Understanding the dynamic behavior of distillation columns," *Ind. Eng. Chem. Res.,* vol. 27, pp. 1848–1862, 1988.
[64] G. Gu, S. Banda, and A. Sparks, "An overview of rotating stall and surge control for axial flow compressors," in *Proc. IEEE Conf. Decision Control*, Kobe, Japan, 1996, pp. 2786–2791.
[65] "Application guideline for centrifugal compressor surge control systems," Release Version 4.3, Gas Machinery Research Council, Southwest Research Institute, Apr. 2008.
[66] H. J. Weigl, J. D. Paduano, L. G. Frechette, A. H. Epstein, E. M. Greitzer, M. M. Bright, and A. J. Strazisar, "Active stabilization of rotating stall and surge in a transonic single stage axial compressor," *J. Turbomach.*, vol. 120, pp. 625–636, 1998.
[67] J. Bailieul, S. Dahlgren, and B. Lehman, "Nonlinear control designs for systems with bifurcations with applications to stabilization and control of compressors," in *Proc. IEEE CDC 34,* New Orleans, Dec. 1995, pp. 3062–3067.
[68] K. O. Boinov, E. A. Lomonova, A. J. A. Vandenput, and A. Tyagunov, "Surge control of the electrically driven centrifugal compressor," *IEEE Trans. Ind. Applicat.,* vol. 42, pp. 1523–1534, Nov./Dec. 2006.
[69] J. S. Orme, J. C. DeLaat, R. D. Southwick, G. W. Gallops, and P. M. Doane, "Development and testing of a high stability engine control (HISTEC) system," in *Proc. 34th AIAA/ASME/SAE/ASEE Joint Propulsion Conference and Exhibit,* NASA/TM-1998-206652, Cleveland, July 1998.
[70] W. K. Lord, D. G. Macmartin, and T. G. Tillman, "Flow control opportunities in gas turbine engines," in *Proc. AIAA 2000-2234 Fluids 2000 Conf. Exhibit,* Denver, June 2000.